

Haemodynamics in a 3D 90-degree Bifurcation

Stevin van Wyk*, Lisa Prah Wittberg*, and Laszlo Fuchs*

1 Linné FLOW Centre KTH Mechanics, Royal Institute of Technology, Stockholm SE-100 44, Sweden, stevin@mech.kth.se

Abstract

The transport behaviour of the haematocrit in the larger arteries is important in defining the variations in viscosity of blood. In this study, a finite volume method is used in order to simulate the blood flow and haematocrit transport through a large 3D human-like 90-degree bifurcation. The simulations are carried out to investigate the importance of explicitly modelling the non-Newtonian viscosity of blood regarding defining the flow. It is expected to be especially important in the regions surrounding a bifurcation. The main focus is to compare non-Newtonian to Newtonian behaviour of the flow through important parameters such as pressure losses, mean viscosity variations and bulk transport properties of haematocrit. The study considers a broad range of physiological and pulsatile flow conditions, and displays the importance of modelling blood flow as a non-Newtonian fluid. The results have a relevant impact regarding the possible discrepancies in important physiological parameters such as wall shear stress (WSS), when coupling the haematocrit field data back to the viscosity models.

Keywords: Haemodynamics, Blood, Biomechanics, CFD, Bifurcation.

Introduction

The role of the complex viscous behaviour of human blood on the haemodynamic conditions of the cardiovascular system is important. A good example is the development and progression of cardiovascular diseases such as coronary thrombosis, which is strongly influenced by the viscous properties [5, 13] and the local distribution and interaction of Red Blood Cells (RBC) and Platelets. Platelet transport towards and deposition on the vessel wall, fundamental to plaque formation in coronary atherosclerosis [4, 31], have been strongly related to blood vessel shear rate and haematocrit [1, 41]. The increased fluid shear increases the rotation of the RBC and thereby hypothesised to enhance platelet diffusivity [28]. An increase or decrease in volume fraction haematocrit on the other hand has been reported to displace or expell platelets, more or less respectively, to the cell poor fluid volumes [1, 23]. Sites of plaque formation that lead to thrombosis are common in the region of the larger 90-degree arterial branches in man. Understanding of two-phase mechanisms in blood, RBC and plasma, is therefore important in prediction and possible control of platelet deposition. Re-atherogenesis is shown to play an important role in the failure of vascular implants such as vascular grafts, artificial hearts, heart valves and ventricular assist devices [21, 32, 38, 39, 43].

Over the years several non-Newtonian models have been developed to account for the shear thinning properties of blood, with respect to two main parameters, shear

rate and volume fraction haematocrit. The models are all steady state models, calibrated for ranges of fixed pressure gradients that defines the range of fixed shear rates in viscometers. The parameters are fixed by bulk macroscopic measurements and not by the microscopic suspension properties. This means that the effective viscosity defined is not an intrinsic property of the suspension, rather a property dependent on specific flow conditions and the averaging of the instrument used to measure [2, 3]. However, due to observations made during this study, it is believed that these models may define important flow field data in physiologically relevant flows; i.e. global parameters, such as pressure drop and mean transport properties of RBCs.

In this study, the temporal and spatial variations of the flow, local viscosity and haematocrit for pulsatile blood-like non-Newtonian fluid properties, in a 90-deg bifurcation, are investigated. Comparisons with Newtonian cases offer a measure for non-Newtonian behaviour of the blood if one assumes that the blood can be considered as a homogeneous mixture characterized by a mixture viscosity. Simulations are carried out with three pulsatile inflow cases, resembling varying load conditions in the human circulatory system, applied to the 3D 90 degree bifurcation geometry. Few studies of this kind have been presented in the past. To be discussed are the effects of pulsation frequency, RBC mass diffusivity, boundary conditions and viscosity on the effects of internal haemodilution (i.e. RBC concentration variations due to shear). The RBC concen-

tration is modelled via a scalar transport model that can be coupled back to the viscosity models.

Methods

Theoretical Background

Viscosity Models

In this study, four different models have been implemented in order to quantify the dynamic viscosity (μ) of Human blood. The chosen models are identified as the most comprehensively developed and widely used, accounting for important behavioural parameters such as the existence of shear strength (shear stress required to initiate flow), Newtonian viscous limits, shear rate dependency and its dependency on cell and molecular composition [12, 44]. Three of the models are functions of both haematocrit and shear rate, while the fourth is a function of solely the latter property.

The Bird-Carreau model, initially developed for reaction kinetics of polymers and similar to a model postulated by Cross [17], describes the viscosity by the following equation [9, 27, 40]:

$$\mu = \mu_{\infty} + (\mu_0 - \mu_{\infty})[1 + (\lambda\dot{\gamma})^2]^{\frac{n_C-1}{2}} \quad (1)$$

Where $\mu_0 = 0.056 Pa.s$ represents "zero shear viscosity", the viscosity value just before the fluid comes to rest; $\mu_{\infty} = 0.00345 Pa.s$ is the Newtonian viscosity or "infinite shear viscosity", the viscosity value at high shear rates, $\lambda = 3.313s$ is the relaxation time constant for haematocrit and n_C is the power law index defining the degree of non-Newtonian behaviour and $\dot{\gamma}$ is the rate of shear of the flow (the same definition in each model). The Bird-Carreau model has been widely used in literature using the constant values as displayed above. It represents the widest range of shear rates of the four models since it reduces to a finite viscosity value at zero shear rate. The major disadvantage is that no explicit haematocrit dependency is defined.

The Casson model, initially derived to describe the flow behaviour of printing ink, was adapted to describing blood viscosity as follows [10, 12]:

$$\mu = \frac{\tau}{\dot{\gamma}} \quad (2)$$

$$\frac{\tau}{\dot{\gamma}} = \frac{[\sqrt{k_C(H)\dot{\gamma}} + \sqrt{\tau_y(H)}]^2}{\dot{\gamma}} \quad \text{for } \tau > \tau_y(H)$$

$$\dot{\gamma} = 0 \quad \text{for } \tau \leq \tau_y(H) \quad (3)$$

Where τ is the fluid shear stress. Terms $k_C(H)$ and $\tau_y(H)$ are a functions of haematocrit H as follows:

$$k_C(H) = \frac{\mu_p}{(1-H)^A} \quad (4)$$

$$\tau_y(H) = \left[\frac{B}{A} ((1-H)^{A/2} - 1) \right]^2 \quad (5)$$

Where μ_p and H represent the blood plasma viscosity and fraction haematocrit, respectively, values for which are displayed in Table 1. The Casson intrinsic viscosity, $k_C(H) = 0.003 Pa.s$ and Shear strength, $\tau_y(H) = 0.0053 Pa$, are both functions of haematocrit, defined according to experimental data for human blood. Constants A and B represent sets of grouped experimental constants defined in work by Cocklet et al. [15], where $A = a\beta$ and $B = a\alpha_B - 1$. The values of the constants are evaluated according to experimental data and can be used to compute the above values for $k_C(H)$ and $\tau_y(H)$. [15, 34, 35]. The model is valid over a wide range of shear rates, however, the shear rate needs to be only greater than $1 s^{-1}$ [12, 45].

One of the most recently developed models is that of the Quemada constitutive equation, known to represent the broadest range of shear rates for blood, greater than approximately $0.01 s^{-1}$ [45]. It was developed to describe the Newtonian viscosity of concentrated particle suspensions through the following equation [36]:

$$\mu = \mu_p \left(1 - \frac{k(\dot{\gamma}, H)}{2} H \right)^{-2} \quad (6)$$

Where $k(\dot{\gamma}, H)$ is a function of the haematocrit, μ_p is the blood plasma viscosity and H is fraction haematocrit, for which blood values are quoted in Table 1. Here $k(\dot{\gamma}, H)$ incorporates the shear rate and haematocrit dependencies as follows [37]:

$$k(\dot{\gamma}, H) = \frac{k_0 + k_{\infty}(\dot{\gamma}/\dot{\gamma}_C)^{1/2}}{1 + (\dot{\gamma}/\dot{\gamma}_C)^{1/2}} \quad (7)$$

$$\dot{\gamma}_C = e^{(-6.1508 + 27.923H - 25.6H^2 + 3.697H^3)} \quad (8)$$

$$k_0 = e^{(3.874 - 10.41H + 13.8H^2 - 6.738H^3)} \quad (9)$$

$$k_{\infty} = e^{(1.3435 - 2.803H + 2.711H^2 - 0.6479H^2)} \quad (10)$$

Where parameters $\dot{\gamma}_C$, k_0 and k_{∞} are the critical shear rate and non-dimensional intrinsic viscosities related to low and high shear rates, respectively. These correlations have been developed by Cokelet et al. [14].

The Walburn and Schneck model is an optimised power law model that includes the important dependencies on shear rate, haematocrit and plasma protein concentration [42]. Equation 11, below, displays its form.

$$\mu = C_1 e^{C_2 H} e^{C_4 \frac{TPMA}{H^2}} \dot{\gamma}^{-C_3 H} \quad (11)$$

Here the empirical constants are $C_1 = 0.000797 Pa.s$, $C_2 = 0.0608$, $C_3 = 0.00499$, $C_4 = 14.585 l/g$. Haematocrit is defined as a percentage and $TPMA = 25 g/l$ is the total proteins minus albumin concentration for human blood. The shear rate validity for this model has been reported as being in the range greater than approximately $0.01 s^{-1}$ [45]. Figure 1 plots the profiles of each model.

Each of the non-Newtonian models described above are implemented with respect to corresponding shear rate validity limits mentioned. All constant material parameters used during this investigation for blood, and the Newtonian fluid, Water, are described in Table 1. The Newtonian

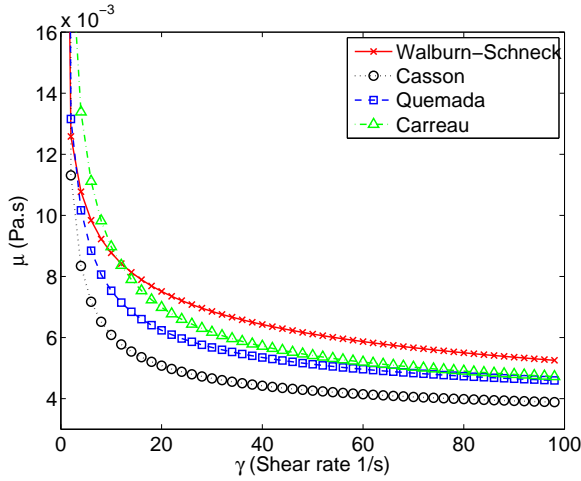


Figure 1 non-Newtonian viscosity models at 45% Haematocrit

value of viscosity for blood is that commonly found to be the lowest viscosity for blood at normal levels, approximately 3.5 times that of water. Whole blood composition (i.e. all components of the blood) at normal levels contains on average approximately 45% haematocrit [7, 18, 33].

Table 1 Material properties for Human Blood at 37 °C and Water at 20 °C

Material	Density (kg/m^3)	Newtonian Viscosity ($Pa.s$)
Whole blood	1060 [8, 18]	0.0035 [7]
Blood plasma	1025 [7]	0.00132 [7]
Water	998.2	0.001

RBC Mass Diffusivity

The mass diffusivity of RBCs and other macro-cells is a consequence of several factors such as fluid shear, electrostatic forces and collisions. There are few studies available that quantify this property. The mass diffusivity of RBCs in concentrated suspensions is enhanced by the flow [6, 11, 24, 26, 29, 30] and constrained by close packing of neighbouring particles [16]. All studies only consider steady flow conditions in simple tube geometries and define empirical shear induced relations describing enhanced diffusivity properties of RBCs [6, 11, 24]. The values determined via these experimental studies are approximately two orders of magnitude greater than Brownian diffusion estimates. However, higher values could be expected during pulsatile flows in complex bifurcating domains. Here complex flow shear patterns, due to strong secondary flow, could further enhance diffusion. It is not yet known how transport properties of blood are affected in the region of bifurcations. Therefore, in this study, a wide range of values are considered in order to represent the possible values

for diffusivity that could occur in these regions of the arterial network.

Governing Flow Equations

The flow of both the Newtonian and non-Newtonian fluids are modelled in the single phase incompressible formulation of the Navier-Stokes equations. The fluids are defined as homogeneous mixtures and expressed as:

$$\frac{\partial u_i}{\partial x_i} = 0 \quad (12)$$

$$\frac{\partial u_i}{\partial t} + u_j \frac{\partial u_i}{\partial x_j} = -\frac{1}{\rho} \frac{\partial p}{\partial x_i} + \nu \frac{\partial^2 u_i}{\partial x_j^2} \quad (13)$$

where $\nu = \mu/\rho$ is the kinematic viscosity. The dynamic viscosity, μ , defined through each of the non-Newtonian models, is normalised by the constant density, ρ , defining the RBC phase as having the same density as the carrier phase.

The haematocrit is modelled as an advected mixture, along with Fick's laws of diffusion, taking the form of a scalar or mass transport equation. This model uses the flow field defined by the flow equations discussed above as its advector. This form of the transport equation and mass conservation are expressed respectively as:

$$\frac{\partial H}{\partial t} = D_H \frac{\partial^2 H}{\partial x_j \partial x_j} - u_j \frac{\partial H}{\partial x_j} \quad (14)$$

Where H is the haematocrit or local volume fraction of the mixture and D_H is the mass diffusivity co-efficient thereof. The range of mass Diffusivity studied is quoted as a range of Schmidt numbers (Sc) in order to assess its influence on the possible RBC range of diffusivities. In equation 14, for mass conservation of the scalar, the left-hand side describes the change over time of the enclosed volume and the right-hand side considers the sum of advective and diffusive fluxes across the boundaries.

Characteristic velocity (U_0 - peak inlet velocity), length (D , main branch diameter), time (ω , angular frequency) and the average inlet volume fraction (\bar{H}) scales can be assigned to non-dimensionalise the mass transport equation, as follows:

$$\frac{4\alpha^2}{Re} \frac{\partial H^*}{\partial T} = \frac{1}{Pe} \frac{\partial^2 H^*}{\partial x_j^{*2}} - u_j^* \frac{\partial H^*}{\partial x_j^*} \quad (15)$$

Where $H^* = H/\bar{H}$, $T = \omega t$, $u_j^* = u_j/U_0$ and $x_j^* = x_j/D$. The non-dimensional terms, Reynolds number, Re , Womersley number, α , Peclet number, Pe and Schmidt number, Sc , can be written as:

$$Re = \frac{U_0 D}{\nu} \quad (16)$$

$$\alpha = \frac{D}{2} \sqrt{\frac{\omega}{\nu}} \quad (17)$$

$$Sc = \frac{\nu}{D_H} \quad (18)$$

$$Pe = ReSc \quad (19)$$

The Womersley number represents the relative importance of transient inertial forces versus the viscous forces. The Reynolds number relates the convective inertial forces to the viscous forces. The combination of these two numbers determines the time dependent flow properties. The Schmidt number is a measure of the rate of viscous diffusion to the rate of mass diffusion of a species in the flow. Mass diffusion here considers only that due concentration gradients. The Peclet number is a measure of dominance of advection of the species with respect to diffusion.

Numerical Methods and Case Set-up

Numerical Methods

A finite volume scheme is employed to discretize the governing equations to second accuracy. Backward implicit time advancement is employed to evolve the equations in time. A constant time step is used to ensure a time resolved solution along with the constant fulfilment of the CFL condition below 1 at each time-step. The PISO scheme maintains pressure-velocity coupling during each time step, via implementation of the pimpleFoam solver in OpenFOAM-1.6. Each of the fifteen cases require approximately 18 pulsation periods to attain a solution that is independent of the initial conditions.

A mesh consisting only of hexahedral elements is implemented. Three grids are used to investigate whether sufficient grid resolution is attained. Consecutively finer grid resolutions; 475 179, 1 410 945 and 4 818 447, respectively, are created for the geometry displayed in Figure 3. The numerical grids are extended at the outlet positions displayed in Figures 3 and 5, in order to improve the description of the development of the haematocrit in the region of the daughter branch and the bifurcation. Here backflow at the outlets, without the extensions, would lead to unrealistic, uniform distribution values entering the region of interest. The actual distribution is highly non-uniform. The averaged element size for each of the three grids are related as follows; $h_2/h_1 = 1.44$ and $h_3/h_2 = 1.51$. Sufficient mesh resolution is attained with grid two of element size 1 410 945, when considering the velocity field. Care has also been taken in defining a high enough resolution in the core of the daughter branch to model the gradients important to the scalar transport model. Grid three mentioned above (cell size 4 818 447), is a local hex refinement of grid two in the region V1. It is therefore also used to evaluate the accuracy of chosen grid two in modelling the scalar transport gradients. Figure 2 shows that no further refinement of grid two is required when analyzing absolute haematocrit values and dilution behaviour, during systole, displayed at the top and bottom respectively. The Bird-Carreau non-Newtonian model is chosen to test this accuracy. Error of the order of 4% for the absolute value plot at $x/d=0.5$ along the z -axis, depicted at the top of Figure 2, is computed at $t/T \approx 0.24$ just after peak flow. However, this does not

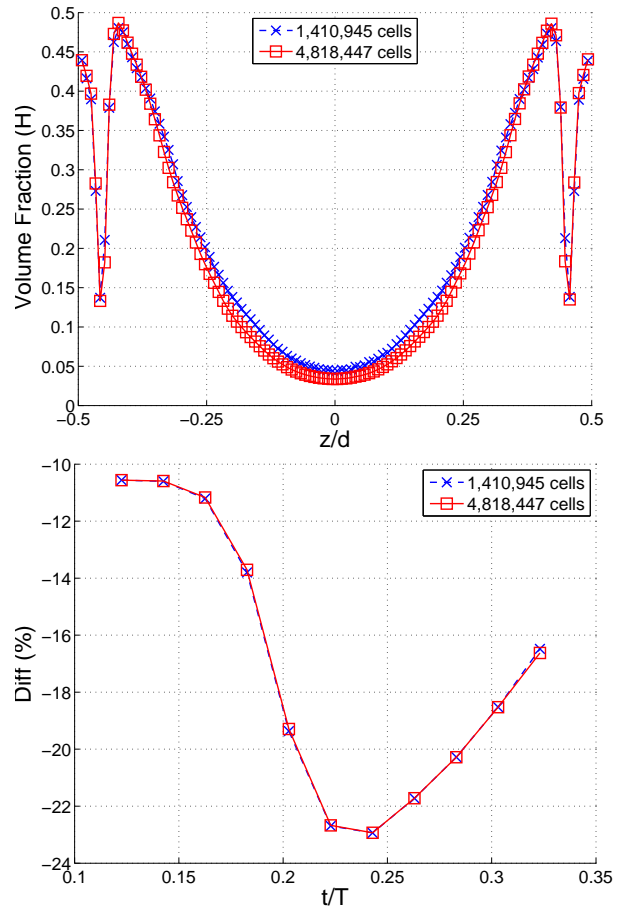


Figure 2 (top) Volume fraction haematocrit (H) line plot along the z -axis of a daughter branch cross-section at $x/d=0.5$ and $t/T \approx 0.24$, as depicted in Figure 5.; (bottom) Percentage difference between average haematocrit in V1 and the inlet from $t/T= 0.1$ to 0.3

significantly affect the dilution in V1, as an error of approximately 0.5% is computed during systole, depicted at the bottom of Figure 2. The error estimate is defined as the RMS of the differences, normalised by the range of values as follows:

$$Error = \sqrt{\frac{\sum_{i=1}^n (\phi_{1,i} - \phi_{2,i})^2}{n}}{(\phi_{1,2,max} - \phi_{1,2,min})} \quad (20)$$

where ϕ is the property and n is the number of samples.

Computational Geometry and Boundary Conditions

A simplified arterial model is chosen in order to avoid patient specific models. It is a simplified model resembling one of the larger arterial branches in humans adequate for understanding general flow behaviour [20]. The geometry consists of a main branch with a diameter, $D = 13.2$ mm and a daughter branch with diameter, $d = 9.35$ mm. The 90-degree bifurcation has a smooth, arterial like shape with an approximate radius of curvature of 9.7 mm, allow-

ing for a time-dependent point of separation. The geometry in question is shown in Figure 3.

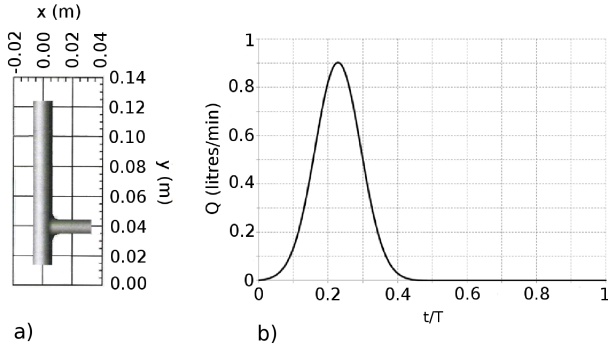


Figure 3 a) Geometric domain with absolute dimensions, b) Intel flow rate vs. Time

The choice of inflow boundary conditions, displayed in Table 2, are chosen according to characteristic arterial flow data common to the abdominal aorta and its larger branches [7]. Peak Inflow velocity or amplitude is estimated from this data. The range of periodic pulsation rates (heart rates), characteristic of arterial flows, are chosen according to a normal range representative of the in-vivo flow conditions in humans. As argued for the geometric choice, a well-defined temporal inflow profile is chosen in order to define this periodic pulsating character [19, 20].

$$Q_{INLET} = A_{MB} \cdot U_0 \cdot e^{-0.5c^2} \quad , \quad c = \frac{t - nT}{0.6T} - 0.38 \quad (21)$$

Where n is the number of preceding periods; i.e. for the first period $n = 0$, the second $n = 1$, etc. U_0 is the peak inlet velocity determined by the present Reynolds number, T is the period time, determined by the present Womersley number, and A_{MB} is the cross-sectional area of the main branch. The inlet flow rate vs. time is plotted in Figure 3 above for the inflow case investigated during this study.

Further boundary conditions implemented are no-slip conditions at the walls and constant reference pressures at the two outlets. The walls are modelled as rigid structures.

Regarding the scalar transport modelling, the inlet boundary conditions implemented are chosen to maintain a constant average Haematocrit, H , that is transported with each of the flow fields. Two profiles are chosen with different Haematocrit values at the walls while maintaining a constant average, shown in Figure 4. The profiles are modelled from experimental high volume fraction RBC profile measurements for laminar flows in tubes [1]. This is typical behaviour of RBCs where the RBCs migrate away from the walls in tube flow due to wall effects [22, 25]. A hyperbolic tangent equation describes this migration in tube flow, leaving a cell depleted plasma layer at the wall. The equation takes the form as follows:

$$H = \tilde{H} (1 + \tanh [m(r - \delta)]) + H_w \quad (22)$$

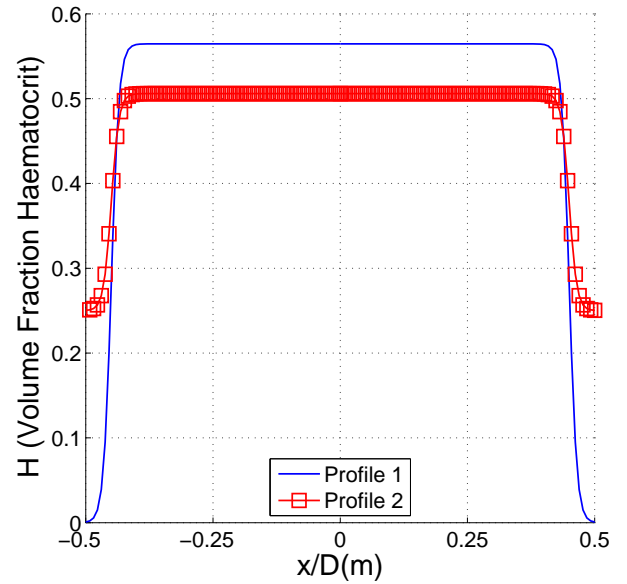


Figure 4 Implemented Haematocrit inlet profiles

Here \tilde{H} is a value chosen to achieve a target bulk haematocrit of 45%, H_w is the haematocrit value set at the wall, r is the radial co-ordinate, m and δ are chosen to set the profile of the distribution towards the wall.

Each of the inlet haematocrit profiles maintain the zero gradient conditions to co-incide with that set at the walls. The volume field condition is initialized with the same average value of 45% as that at the inlet. Zero gradient conditions are also stipulated at both outlets.

Data is acquired after several periods depending on each flow case. The convergence criteria used for this study was that the volumetric difference in mass in the region of interest V2, from cycle to cycle, not to change by more than 1%.

Case Setup and Analysis

Three inflow cases are defined to which each of the Newtonian and non-Newtonian viscous models are applied. Each case has the same peak inflow velocity but differ in pulsation time, shown in Table 2. The range of pulsation time, presented as beats per minute (BPM), represents a range of physiological human heart rates, depending on the individual and degree of effort. Reynolds and Womersley numbers for blood are quoted as maximum and minimum values respectively, regarding the minimum viscosity for blood quoted in Table 1.

For each of the flow cases the scalar transport model, representing the transport properties of RBC as a mixture, is computed. The flow is described as homogenous. That is, the RBC mixture phase or haematocrit has the same density as the carrier fluid. The haematocrit, however, is defined as occupying a certain volume fraction of the fluid volume representing the mass of RBC. A species equation, equation 14, is used to model the mass diffusion and advection of the haematocrit as a volume fraction value. This equation is coupled back to the computed flow field (u_j).

Table 2 Case set up parameters. Peak inflow velocity, heart beats per minute (BPM), max (Re) and min (α).

	Peak Inlet Velocity	BPM	Re	α
case 1	0.11	30	440	6.5
case 2	0.11	60	440	9
case 3	0.11	90	440	11

Three RBC mass diffusivities are considered for each inflow case, represented by a range Schmidt numbers defined with respect the viscosity of water, an order of magnitude apart, $Sc \approx 1.1, 11, 110$. As stated earlier, experimental values for mass diffusivity of RBCs in complex shear flow cases does not exist in literature.

The presentation of results will refer to Table 2 when case referencing. The Newtonian reference case is used to obtain a measure of non-Newtonian behaviour and aims to show that the effects are not simply caused by an increase or decrease in Newtonian viscosity. The similarities in bulk behaviour displayed between the non-Newtonian models offers qualitative information regarding blood like mass transport phenomena.

The main region of interest, located by the shaded region in Figure 5, is due to secondary flows that influence transport properties, forming a notable separation bubble due to the 90-degree deviation in the flow. Reference dimensions and sample regions used in representing the analysed data are illustrated in Figure 5.

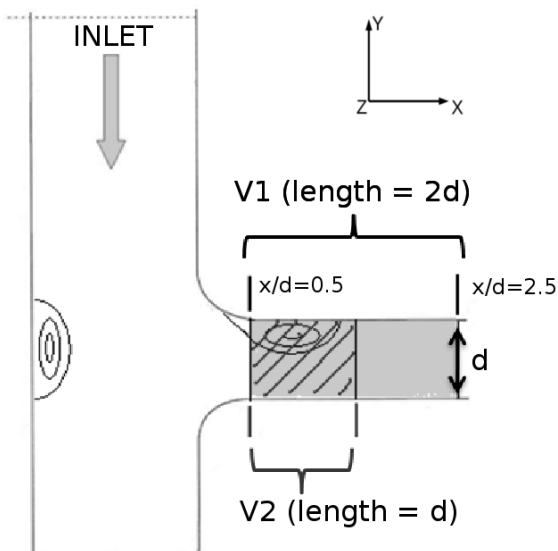


Figure 5 Co-ordinate system and region references

Volumetric data is extracted from the designated regions of interest, V1 and V2, regarding pressure gradients, viscosity and volume fraction haematocrit variations. Effects of pulsation frequency, RBC diffusivity and the distribution profile on the haemodynamic properties are presented. One-way and two-way coupled field dependencies

are also compared. Region V2 is half the volume of region V1, focused on the separation bubble. It is chosen to quantify the influence, proportion wise, the separation bubble has on haematocrit variation in region V1.

Results

The results presented in the following sections will focus on the differences in transport properties for an RBC mixture using Newtonian and non-Newtonian viscosity models. Firstly, the differences non-Newtonian viscosity models share when describing blood-like flow behaviour will be discussed. The effects of RBC mass diffusivity, pulsation frequency, inlet boundary conditions (Profile 1 and 2) and the different viscosity models on transport properties in V1 will be displayed. Finally, the influence of the separation bubble on the change in haematocrit in region V1 is analysed relative to variations in region V2.

Pressure losses and Viscosity variation

Mean field pressure gradient variations, representing pressure losses, for region V1 for all non-Newtonian models relative to water are depicted in Figure 6. Mean pressure gradient values for case 1 initially show a sharp increase, becoming larger than that of water. This coincides with the initial high mean levels in viscosity and an increasing flow rate during systole, Figure 7. The maximum differences in peak pressure gradient around $t/T \approx 0.18$ are approximately 20% for between the Bird-carreau and Casson models. During this increase in flow rate to the point of peak systole the pressure gradient tends to be higher than for water. Almost immediately after the peak pressure gradient a sudden drop takes place for all cases, reaching a minimum just after peak systole before rising again. This also coincides with the minimum mean viscosity where the shear rates are highest. From this point onwards much lower pressure gradients exist compared to water for case 1. Case 3 continues to rise from the point just after peak systole at $t/T \approx 0.24$, where pressure gradients are lower than that of water, to $t/T \approx 0.32$ where higher pressure gradients than that of water peak again. From this point onwards there is a drop again, until $t/T \approx 0.5$ where the pressure gradient is slightly lower than water. Around $t/T \approx 0.7$ the pressure gradients begin to resemble that of water as the blood comes to rest or exhibits minimal motion. Thereafter the pressure gradient differences almost disappear as flow ceases during diastole. In general, during the pulsation cycles for all frequencies, large differences in pressure gradient are observed between the non-Newtonian viscosity models and the Newtonian model water.

The viscosity variation plots displayed in Figure 7 show that as the flow rate increases during systole, all the models and cases reach a minimum at peak inflow, $t/T \approx 0.22$. As the flow rate decreases the viscosity increases again until a point at $t/T \approx 0.55$ for case 1 and $t/T \approx 0.7$ for case 2. There is no distinct point at which a peak is reached in case 3, as the subsequent decrease seen in case 1 is due to reverse flow. As the pulsation fre-

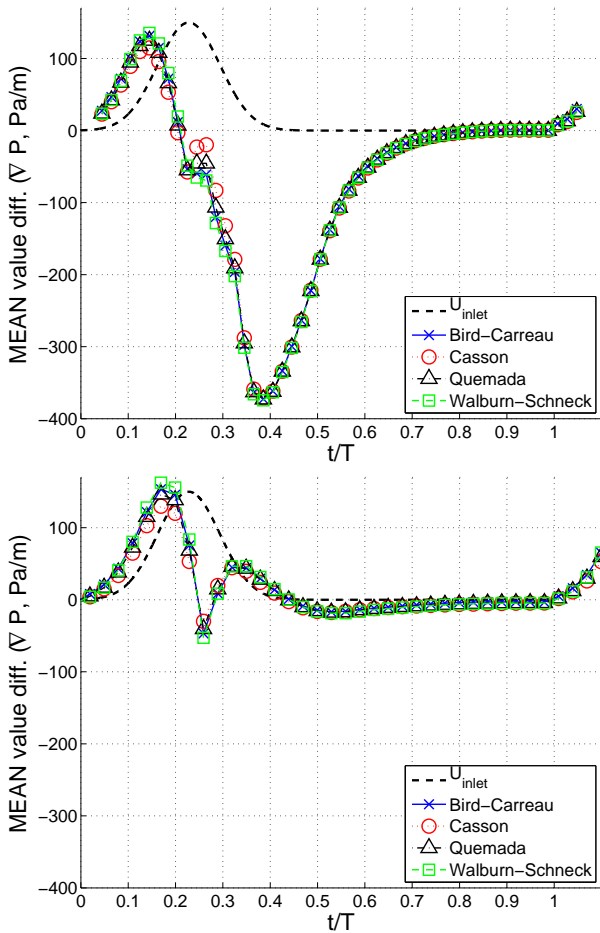


Figure 6 Difference in the mean pressure gradient (∇P) for all non-Newtonian models minus the pure Newtonian case (Water) for (top) Case 1 and (bottom) case 3.

quency increases reverse flow in region V1 decreases and takes place for a shorter period of time at 90 bpm. It is also observed that each of the viscosity models exhibit very different peaks in viscosity. This is due to the validity limits set for each model that are constrained differently at shear rates less than 1 s^{-1} . The reason for the Bird-Carreau model to display the highest mean viscosity is due to being the only model valid for the full range of shear rates, including zero shear rate. The results presented in this section displays the importance of describing the fluid, blood, as non-Newtonian in character. The non-Newtonian flow behaviour is therefore more important than a simple increase or decrease in viscosity and will describe vastly different transport behaviour than a Newtonian fluid like water would.

Dilution characteristics

The dilution characteristics are quantified as the temporal variation of the average haematocrit fraction in region V1 minus the inlet average. In all figures the dilution variation is displayed as a percentage difference or deviation with reference to inlet profile 1. Large variations are observed in the region of the daughter branch when advection dom-

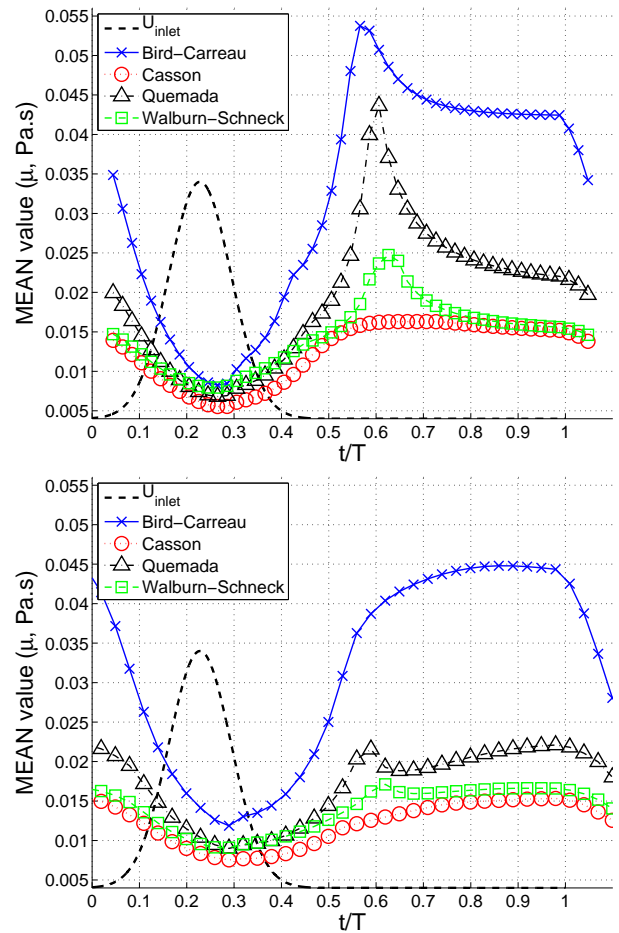


Figure 7 Difference in mean field viscosity (μ) quantities for all non-Newtonian models in region V1 for (top) Case 1 and (bottom) Case 3.

inates i.e. at high Schmidt numbers. The highest Schmidt number investigated during the study is 110 for which diffusion is observed to be very low. In the region of bifurcations, flow features such as separation and secondary flows cause these large variations due to shear. Early on in the pulsation cycle the centrifugal effect, characteristic to the radius of the bifurcation curvature, leads to the flow separation and generates secondary vortices. The shear layers produced by these secondary flows leads to the mass transport behaviour affecting haematocrit dilution in the region of bifurcations.

Figure 8 shows the progression of dilution for cases 1 and 3 in region V1 as a percentage drop in fraction. In all cases the general progression is similar and correlates with the applied inflow characteristics. However, with increasing pulsation frequency the correlation becomes less. For case 1 the first stage of systole shows an increase in dilution leading to a maximum around peak systole, at $t/T \approx 0.22$, of as high as 22% for the Bird-Carreau model and lowest 16% for the Casson model. For case 3 there is a delay in peak dilution, taking place at around $t/T \approx 0.3$, leading to dilution of 20% and 12% for the same models as in case 1. This is an expected delay for higher Womersley numbers, where the transient inertia is higher leading to a

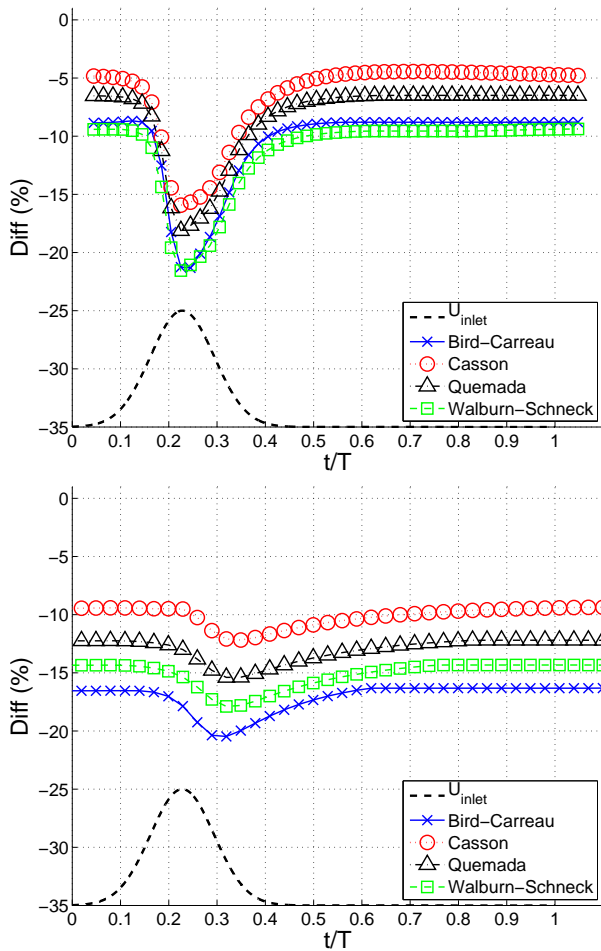


Figure 8 Comparison of mean fraction haematocrit difference in region V1, minus the inlet average, for (top) Case 1 and (bottom) Case 3.

delay in the core flow momentum. Formation of the separation bubble is therefore delayed, due to the flow taking more time to accelerate to a certain velocity. The absolute increase in dilution between systole and diastole for case 1 is larger than that for case 3. Case 1 shows an absolute difference of between 11 and 12% and Case 3 only between 3 and 4%, considering the same viscosity models as earlier. This is caused due to the diminished size of the separation bubble at higher pulsation frequencies. The delay in formation and the shorter pulsation time, decreases the time available for the separation bubble to form. The size of the separation bubble can be depicted by the local extent of negative axial flow (backflow) near the bifurcation, in the daughter branch. Figure 9 displays the axial velocity contours of the Bird-Carreau model at $t/T \approx 0.34$, after systole, when the separation bubble approximately nears its maximum size for all cases. The localised 'bubble' of backflow decreases in size as the pulsation frequency increases. The emphasis or focus on the impact of the separation bubble is described in the section following.

After the peak in dilution, the separation bubble continues to grow during the deceleration stage of systole. A steady decrease in dilution is observed in both cases 1 and

3, eventually reaching a constant bulk haematocrit fraction in the domain. Case 1 reaches this point between $t/T \approx 0.4$ and 0.6 and case 3 between $t/T \approx 0.6$ and 0.8 , depending on the viscosity models. The minimum dilution is therefore attained and ranges between 9% and 5% for case 1

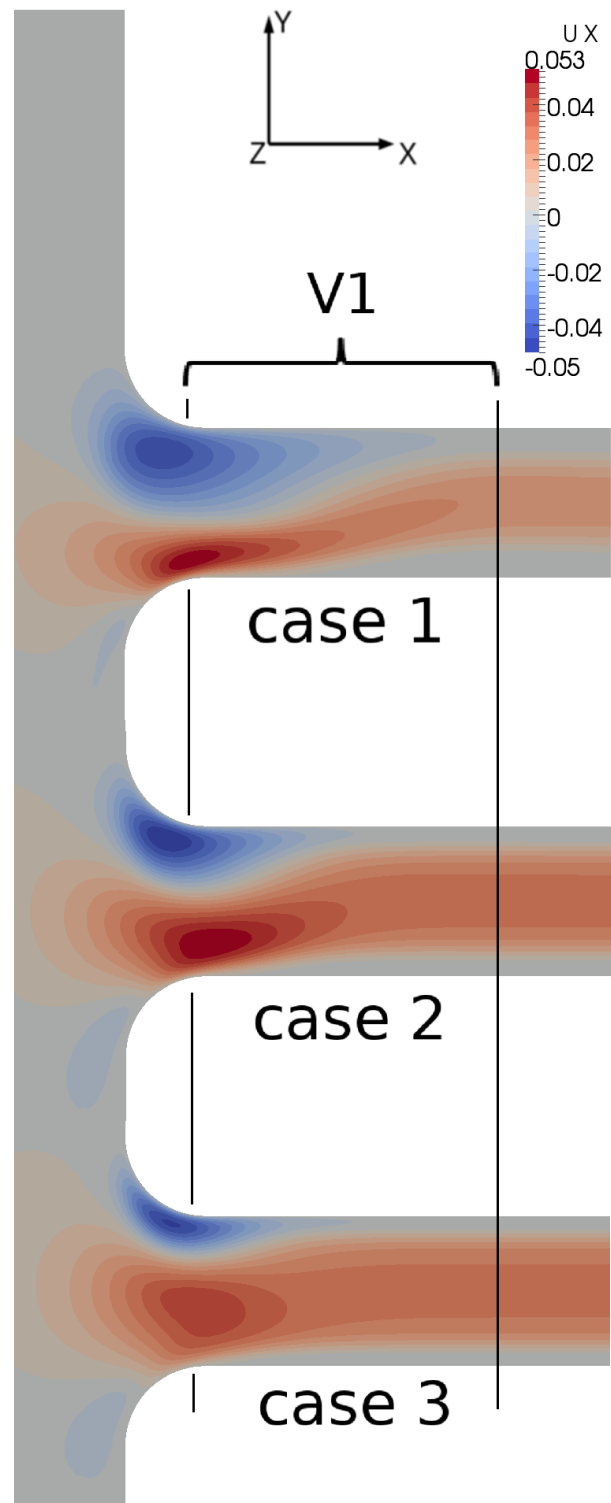


Figure 9 Axial velocity (m/s) contours relative to the daughter branch of all cases for the Bird-Carreau model, at $t/T \approx 0.34$.

and between 16% and 10% for case 3, regarding the Bird-Carreau and Casson viscosity models respectively. The differences in the dilution properties described by the different viscosity models are due to a combination of the differences in their viscosity limits and non-Newtonian behavioural description. However, there is a consistent observation that can be made regarding the extent of dilution through the pulsation cycle. The non-Newtonian model with the consistently highest mean viscosity, as seen in Figure 7, generates the highest levels of dilution. This can be observed for both cases in Figure 8 and is also true when considering the minimums. In general the Bird-Carreau and the Casson models represent the two extremes for maximum and minimum dilution respectively. Models Walburn-Schneck and Quemada always tend to define values between these models and can be seen to be strongly related to the mean viscosity defined in Figure 7. This in turn can be related to the shear layer thickness defined by each viscosity model. A higher mean viscosity is associated with thicker shear layers in the daughter branch.

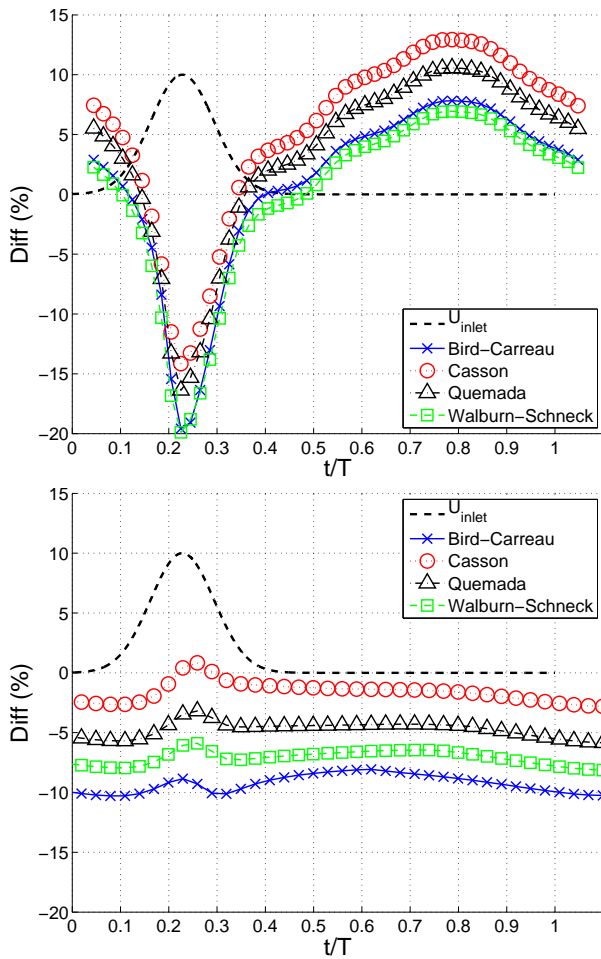


Figure 10 Comparison of mean fraction haematocrit difference in region V1, minus the that defined by water, for (top) Case 1 and (bottom) Case 3.

Another fundamental behavioural property displayed in Figure 7 is the difference in the maximum range of

haematocrit variation or dilution for each viscosity model. As the pulsation frequency increases this range decreases i.e. there is smaller difference between the systolic and diastolic dilution in case 3 than in case 1. This can be explained through equation 15, describing the effect of non-dimensional parameters, Reynolds (Re), Womersley (α) and Schmidt (Sc) numbers, on the transport. The plots in Figure 8 maintain constant Re and Sc , but increase α as the frequency increases. This therefore means that the $\frac{\partial H^*}{\partial T}$ term, which signifies the rate of change in haematocrit over time, decreases and is consistent with what is observed in the results. Another important feature is that case 3 also shows a lower value of dilution during the diastolic phase than case 1, reflected by all the viscosity mod-

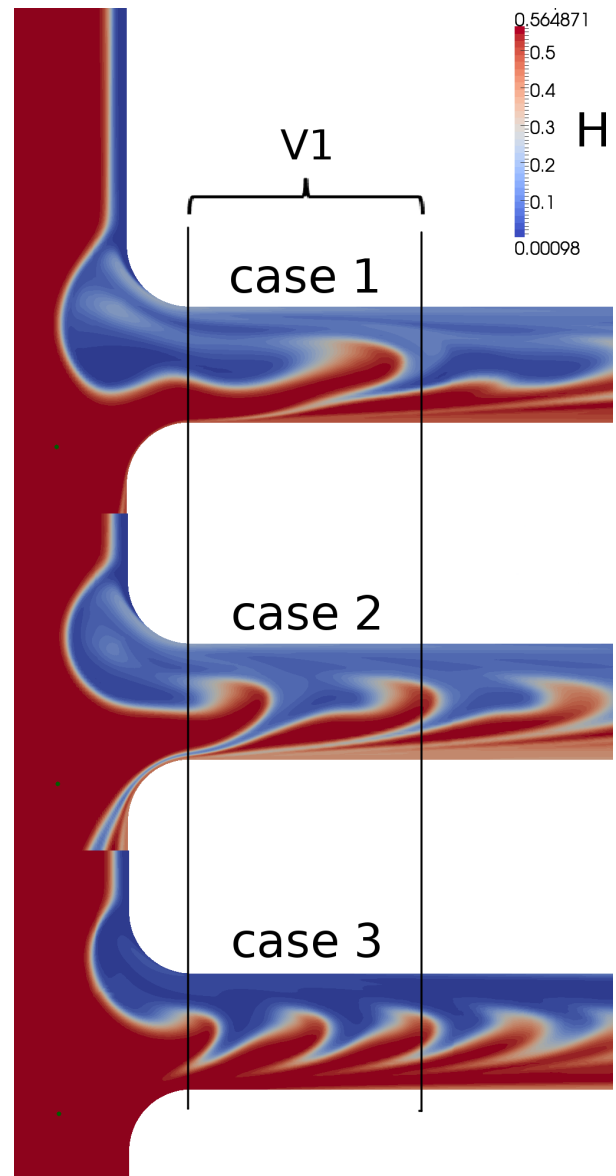


Figure 11 Example of local haematocrit fraction variation for all cases at $t/T = 1$ (end of the cycle), with increasing frequency, focusing on region V1. Data is extracted at the centre channel cross-section, showing the complete bifurcation profile.

els. This can be understood by the above explanation and can be graphically expressed by the number of haematocrit pulses or packets existing in region V1 at any point in time during diastole. Figure 11 uses the Bird-Carreau viscosity model as an example to illustrate the evolution of the pulses of haematocrit with increasing frequency from case 1 to 3 respectively. The diminished size of the separation bubble for increased frequency is also evident, described earlier as one of the main reasons for decrease in the total increase in dilution from the diastolic level.

The impact of defining blood as a non-Newtonian fluid, in order to model its two phase flow properties, is quantified by comparing its dilution behaviour to that of water. Figure 10 displays temporal data of the dilution defined by non-Newtonian models minus the dilution defined by water for case 1 and case 3, in relation to Figure 8. In case 1 it is observed that during diastole ($t/T = 0.4$ to 1) there is a difference in relative dilution. This is due to the flow of water alone, as all non-Newtonian models show no change in dilution during this part of the cycle. The dilution defined by the non-Newtonian viscosity models shows a maximum of between 7 and 13% less compared to water. The reason for this is that water has a relatively low Newtonian viscosity and is observed to maintain momentum in the flow throughout the cycle, since much less force is required to move a volume of fluid. This means that transport properties vary by advection throughout the cycle. In case 3 it can be noticed that the difference during diastole is much less pronounced as compared to case 1. This in turn is due to the same reasons described earlier, referring to equation 15. The non-Newtonian models display greater dilution throughout this part of the cycle, ranging between 1 and 10%.

During the systolic part of the cycle for case 1, between $t/T=0$ and 0.4, there are large differences in dilution. From the start of systole to the peak there is a very steep progression in relative difference, leading to a peak dilution of between 14 and 20%. After peak systole, during the deceleration phase, there is steady decrease in dilution until a constant dilution value is reached again during diastole. This sharp variation in definition of dilution behaviour displays the degree of importance in modelling the two phase flow of blood by non-Newtonian viscosity models.

Influence of Separation Bubble

The smaller region V2 is used in order to focus on the dilution properties surrounding the separation bubble, in order to further quantify the importance of the influence that the separation bubble has on the dilution properties within region V1. At high Schmidt numbers and due to the formation of secondary flows in the daughter branch enhanced dilution behaviour exists.

Figure 12 shows the dilution properties existing in V2, along with a plot depicting its percentage difference relative to region V1. Figure 12 (top) shows that there is a maximum dilution around peak systole as in V1, with

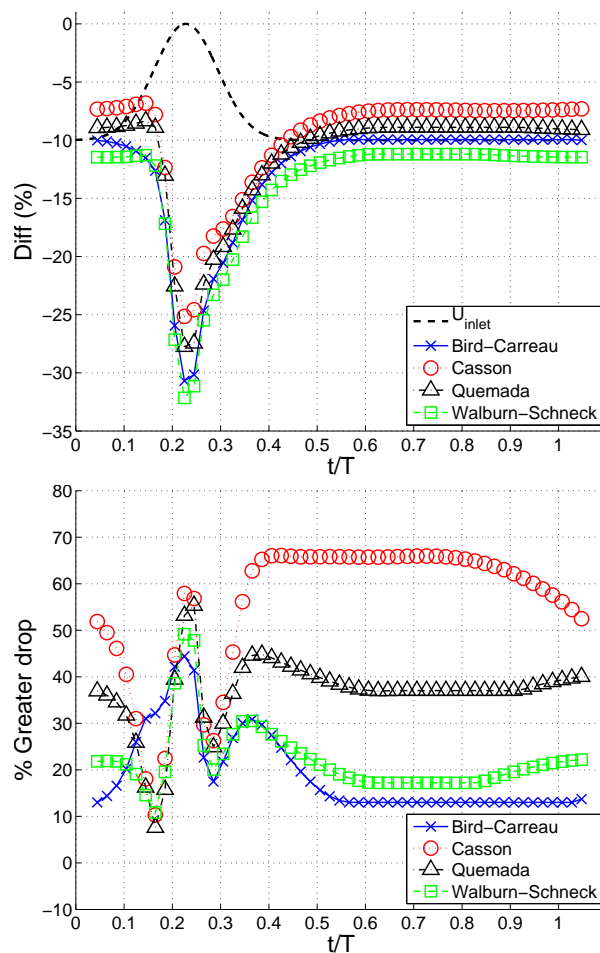


Figure 12 Case 1 (top) mean fraction haematocrit difference in region V2 with respect to the inlet average and (bottom) (%) greater drop in region V2 vcompared to region V1.

a dilution of between 25 and 32%. However, the maximum dilution is 50 to 60% greater as compared to that displayed for V1, depicted in Figure 12 (bottom) denoting the % greater drop. During peak systole, all viscosity models display the same trend, showing the dominant influence of the formation of the separation bubble. At this heart cycle frequency, region V2 shows a constantly high dilution influence, even throughout diastole, depending on the viscosity model. The different viscosity models display a great discrepancy where the Casson model shows an 80% greater drop as apposed to the Bird-Carreau model where there is a constant value of about 10% after systole. The higher value obtained using the Casson model is due to a much lower mean viscosity observed during diastole, compared to that for the Bird-Carreau model, shown in Figure 7. The effect of the flow is a combination of improved mixing and backflow mechanisms for the Casson model and the opposite effect for the Bird-Carreau model, during the transport of haematocrit. When considering the Casson model these effects carry more haematocrit away from both regions, upstream, back towards the junction, thereby further diluting the regions. Hence the greater drop percentage during diastole, than for the Bird-carreau model.

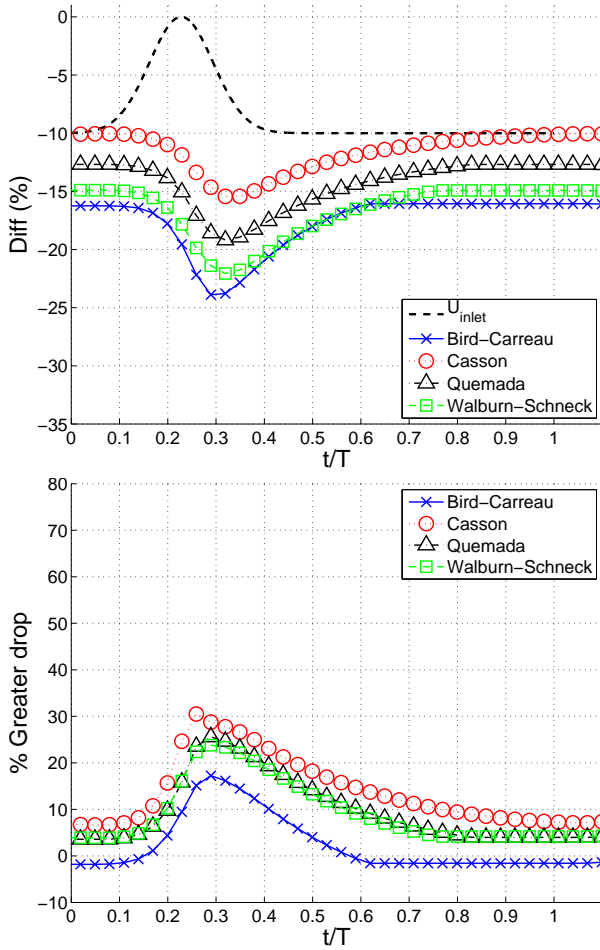


Figure 13 Case 3 (top) mean fraction haematocrit difference in region V2 with respect to the inlet average and (bottom) (%) greater drop in region V2 vcompared to region V1.

For case 3, Figure 13 displays the same form of dilution as for case 1 above. During diastole, when comparing the dilution to that occurring in region V1, there is little difference in the progression from the results displayed in Figure 8. However, there is a peak dilution around $t/T \approx 0.3$ of approximately 15 to 24% appearing during systole where the separation bubble influences the flow. This leads to a reasonably large contribution from V2 to the overall dilution in V1, signified by a 15 to 30% greater drop. Unlike case 1, there is not enough time for the flow to develop enough for mixing and backflow to play a significant role for this heart cycle frequency. The most influential secondary flow mechanism affecting dilution behaviour is the formation of the separation bubble, causing segregated flow patterns which narrows the channel of transport into the daughter branch, during systole.

Effect of RBC profile and Schmidt number

It is of interest to understand the influence the Schmidt number as well as the inlet haematocrit profiles has on the dilution. Moreover, whether or not both RBC inlet profiles produce significant dilution, is interesting when con-

sidering the differences in variation of both Newtonian and non-Newtonian viscosity models. Also, the Sc number for which advective or diffusive fluxes dominate the flow for non-Newtonian viscosity models is as well.

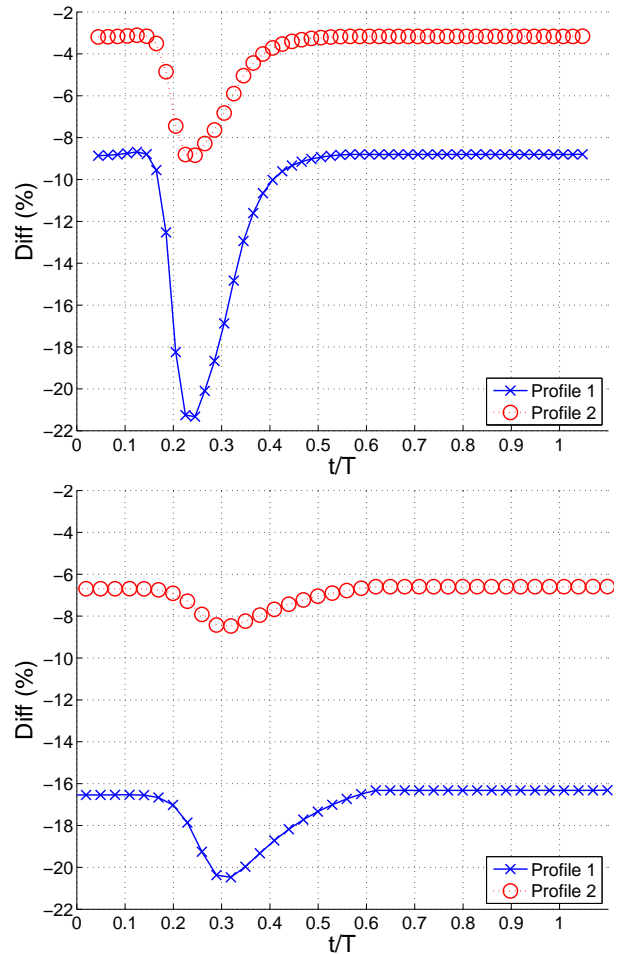


Figure 14 Difference in dilution behaviour of the Bird-Carreau model described by profile 1 and 2 for (top) Case 1 and (bottom) Case 3.

Haematocrit Inlet profile conditions

In Figure 14 the variation of dilution between cases 1 and 3 are compared for both profiles for the Bird-Carreau model. Both cases 1 and 3 display the same trend. The dilution for case 1 shows that there is a difference of 6% between the profiles during diastole and up to 12% difference near peak systole. Considering the dilution for case 3 there is a larger difference between the profiles during diastole of 10% but with a peak systole difference repeatative of case 1. Both profiles describe large, clear variations from what is imposed at the inlet. Since each profile defines the same average inlet haematocrit, the differences in dilution behaviour come from the minimum value at the wall and the gradients inherently defined. The trend described by Figure 14 is similar for all viscosity models.

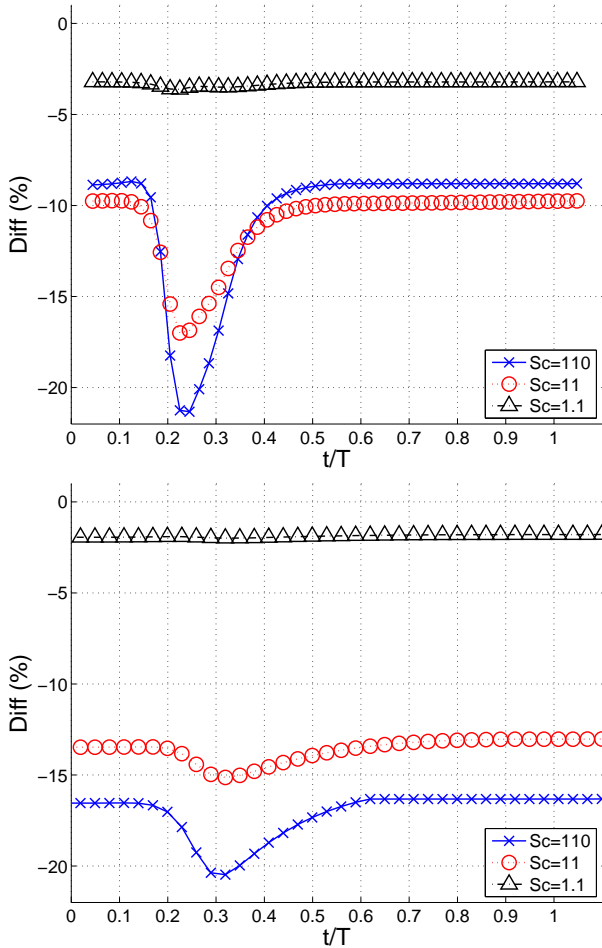


Figure 15 Difference in dilution behaviour of the Bird-Carreau model described by the range of Schmidt number investigated, between $Sc = 1.1$ and 110 (top) case 1 and (bottom) case 3.

Schmidt number variation

The variation of the Schmidt number represents the possibility of the increase in mass diffusivity of the haematocrit when interacting with enhanced secondary flows in the region of the bifurcation. Figure 15 shows the variation haematocrit over a cycle for the three Schmidt numbers studied, using case 1 and case 3, region V1 and the Bird-Carreau model. The dilution is strongly influenced by the increase in Schmidt number. From $Sc \approx 11$ and higher the dilution during diastole is similar around 9 to 10% (1% difference) for case 1, while displaying a larger difference for case 3 of up to 3%. Case 3 shows an additional 4 and 8% increase in diastolic dilution, for $Sc = 11$ and 110 respectively. The higher pulsation frequency means that there are more frequent haematocrit packets generated, causing a greater increase in level of dilution. The higher Schmidt numbers are more important at higher heart pulsation frequencies.

During peak systole the difference between the higher Schmidt numbers, $Sc = 11$ and 110, is as large as 4% for case 1 and 5% for case 3. The difference between the

Schmidt numbers stays similar for all cases. However, the absolute increase in dilution from diastole to systole is still larger for larger values of Sc . This difference is even greater when considering region V2. At low Schmidt numbers, $Sc = 1.1$, the diffusive time scale is small enough, allowing the diffusive flux to penetrate the separation bubble. This means that only a minor variation in dilution during peak systole is experienced. There is, however, a constant dilution value of approximately 3% existing throughout the cycle. As discussed earlier, the haematocrit or the RBCs have a low mass diffusivity in high concentrations and therefore advection dominates the transport behaviour. All viscosity models display similar trends.

Conclusions

This investigation has carried out analysis of flow field and transport behaviour of a blood like fluid. The possible extent of importance of modelling blood in its true character, as a non-Newtonian viscous fluid, is quantified. Data representing pressure losses, viscosity variations and haematocrit transport behaviour has yielded:

- There are large variations in mean pressure gradients and viscosity throughout the heart cycle, at physiological pulsation frequencies between 30 and 90 beats per minute, for all non-Newtonian models relative to the Newtonian model water. This varies throughout the heart cycle for pulses between 30 and 90 beats per minute. Describing the flow from a non-Newtonian viscosity perspective is observed to be more important than a simple increase or decrease in Newtonian viscosity.
- Bulk dilution in the extended region V1 is as high as 16 to 22% in terms of RBC concentration, for case 1, representing low heart pulses of 30 bpm, and 12 to 20% for case 3, representing higher heart pulses of 90 bpm. Large changes in fraction haematocrit therefore exists in a 90 degree branch with respect to the average inlet value.
- Large differences in bulk dilution between non-Newtonian and Newtonian models exists. At peak systole up to 14 and 20% difference can be observed at low heart pulse frequencies of 30 bpm and 10% at higher pulse frequencies. This shows the importance of describing transport properties of haematocrit via non-Newtonian viscosity models.
- The contribution of the separation bubble to bulk dilution behaviour is important. It defines the large variations throughout the heart cycle, especially during systole. Relative bulk dilution increase in region V2 with respect to V1 is as high as 60% near peak systole for case 1 and 30% for case 3.
- The large variations in bulk haematocrit existing at high Schmidt numbers, when comparing non-Newtonian to Newtonian viscosity models, implies

that there should be important influences on viscosity that need to be considered. The viscosity of blood is dependent on local haematocrit fraction.

In future work the haematocrit fraction will be coupled back to viscosity models to define a more complete viscosity dependency. It is then feasible to investigate physiological parameters such as Wall Shear Stress, thought to be important in the development of vascular diseases.

Acknowledgements

The financial support from the Swedish Research Council (Vetenskapsrådet) is greatly acknowledged. Computational resources were provided by the Swedish National Infrastructure for Computing (SNIC) and the High Performance Computing Center North (HPC2N).

References

- [1] P. Aarts, S. Van Den Broek, G. Prins, G. Kuiken, J. Sixma, and R. Heethaar. Blood platelets are concentrated near the wall and red blood cells, in the center in flowing blood. *Arteriosclerosis, Thrombosis, and Vascular Biology*, 8(6):819, 1988.
- [2] H. Barnes. A review of the slip (wall depletion) of polymer solutions, emulsions and particle suspensions in viscometers: its cause, character, and cure. *Journal of Non-Newtonian Fluid Mechanics*, 56(3):221–251, 1995.
- [3] H. Barnes. Measuring the viscosity of large-particle (and flocculated) suspensions—a note on the necessary gap size of rotational viscometers. *Journal of non-newtonian fluid mechanics*, 94(2-3):213–217, 2000.
- [4] H. Baumgartner and C. Haudenschild. Adhesion of platelets to subendothelium. *Annals of the New York Academy of Sciences*, 201(1):22–36, 1972.
- [5] R. Becker. The role of blood viscosity in the development and progression of coronary artery disease. *Cleveland Clinic journal of medicine*, 60(5):353, 1993.
- [6] J. Bishop, A. Popel, M. Intaglietta, and P. Johnson. Effect of aggregation and shear rate on the dispersion of red blood cells flowing in venules. *American Journal of Physiology-Heart and Circulatory Physiology*, 283(5):H1985, 2002.
- [7] J. Bronzino, editor. *The Biomedical Engineering Handbook, second edition*. Boca Raton: CRC Press LLC, 2000.
- [8] D. Brooks, J. Goodwin, and G. Seaman. Interactions among erythrocytes under shear. *Journal of applied physiology*, 28(2):172, 1970.
- [9] P. Carreau. Rheological equations from molecular network theories. *Journal of Rheology*, 16:99–127, 1972.
- [10] N. Casson. *Rheology of disperse systems*. Pergamon Press, London, 1959.
- [11] W. Cha and R. Beissinger. Evaluation of shear-induced particle diffusivity in red cell ghosts suspensions. *Korean Journal of Chemical Engineering*, 18(4):479–485, 2001.
- [12] S. Charm and G. Kurland. Blood rheology. *Cardiovascular fluid dynamics*, 2, 1972.
- [13] Y. Cho and K. Kensey. Effects of the non-newtonian viscosity of blood on flows in a diseased arterial vessel. part 1: Steady flows. *Biorheology*, 28:241, 1991.
- [14] G. Cockett. The rheology and tube flow of blood. *Handbook of Bioengineering*, page 14, 1987.
- [15] G. Cockett, E. Merrill, E. Gilliland, H. Shin, A. Britten, and R. Wells Jr. The rheology of human blood—measurement near and at zero shear rate. *Journal of Rheology*, 7:303–307, 1963.
- [16] E. Cohen and I. De Schepper. Transport properties of concentrated colloidal suspensions. *AIP Conference Proceedings*, 256:359, 1992.
- [17] M. Cross. Kinetic interpretation of non-newtonian flow. *Journal of Colloid and Interface Science*, 33(1):30–35, 1970.
- [18] J. Cutnell and K. Johnson. *Physics, 8th Edition*. Wiley, 1998.
- [19] P. Evengren, L. Fuchs, and J. Revstedt. On the secondary flow through bifurcating pipes. *Physics of Fluids*, 22:103601, 2010.
- [20] P. Evengren, L. Fuchs, and J. Revstedt. Wall shear stress variations in a 90-degree bifurcation in 3d pulsating flows. *Medical engineering & physics*, 32(2):189–202, 2010.
- [21] A. Garatti, G. Bruschi, T. Colombo, C. Russo, M. Lanfranconi, F. Milazzo, M. Frigerio, and E. Vitali. Clinical outcome and bridge to transplant rate of left ventricular assist device recipient patients: comparison between continuous-flow and pulsatile-flow devices. *European Journal of Cardio-Thoracic Surgery*, 34:275, 2008.
- [22] H. Goldsmith. *Red cell motions and wall interactions in tube flow.*, volume 30. Federation proceedings, 1971.
- [23] H. Goldsmith. The flow of model particles and blood cells and its relation to thrombogenesis. *Progress in hemostasis and thrombosis*, 1:97, 1972.
- [24] H. Goldsmith and J. Marlow. Flow behavior of erythrocytes. ii. particle motions in concentrated suspensions of ghost cells. *Journal of Colloid and Interface Science*, 71(2):383–407, 1979.
- [25] H. Goldsmith and S. Mason. Some model experiments in hemodynamics iv. *Theoretical and Clinical Hemorheology, Springer, New York*, pages 47–59, 1971.
- [26] S. Hudson. Wall migration and shear-induced diffusion of fluid droplets in emulsions. *Physics of fluids*, 15:1106, 2003.
- [27] B. Johnston, P. Johnston, S. Corney, and D. Kilpatrick. Non-newtonian blood flow in human right coronary arteries: steady state simulations. *Journal of Biomechanics*, 37(5):709–720, 2004.
- [28] K. Keller. Effect of fluid shear on mass transport

- in flowing blood. In *Federation proceedings*, volume 30, page 1591, 1971.
- [29] M. King and D. Leighton Jr. Measurement of shear-induced dispersion in a dilute emulsion. *Physics of Fluids*, 13:397, 2001.
- [30] D. Leighton and A. Acrivos. The shear-induced migration of particles in concentrated suspensions. *Journal of Fluid Mechanics*, 181(1):415–439, 1987.
- [31] P. Libby, M. DiCarli, and R. Weissleder. The vascular biology of atherosclerosis and imaging targets. *Journal of Nuclear Medicine*, 51:33S, 2010.
- [32] P. Lin, R. Bush, Q. Yao, A. Lumsden, and C. Chen. Evaluation of platelet deposition and neointimal hyperplasia of heparin-coated small-caliber eptfe grafts in a canine femoral artery bypass model. *Journal of Surgical Research*, 118:45–52, 2004.
- [33] G. Lowe, F. Fowkes, J. Dawes, P. Donnan, S. Lennie, and E. Housley. Blood viscosity, fibrinogen, and activation of coagulation and leukocytes in peripheral arterial disease and the normal population in the edinburgh artery study. *Circulation*, 87(6):1915, 1993.
- [34] E. Merrill, E. Gilliland, G. Cokelet, H. Shin, A. Britten, and R. Wells Jr. Rheology of human blood, near and at zero flow:: Effects of temperature and hematocrit level. *Biophysical Journal*, 3(3):199–213, 1963.
- [35] K. Perktold, M. Resch, and H. Florian. Pulsatile non-newtonian flow characteristics in a three-dimensional human carotid bifurcation model. *Journal of biomechanical engineering*, 113:464, 1991.
- [36] D. Quemada. Rheology of concentrated disperse systems and minimum energy dissipation principle. *Rheologica Acta*, 16(1):82–94, 1977.
- [37] D. Quemada. Rheology of concentrated disperse systems ii. a model for non-newtonian shear viscosity in steady flows. *Rheologica Acta*, 17(6):632–642, 1978.
- [38] C. Schmid, T. Tjan, C. Etz, C. Schmidt, F. Wenzelburger, M. Wilhelm, M. Rothenburger, G. Drees, and H. Scheld. First clinical experience with the incor left ventricular assist device. *The Journal of heart and lung transplantation*, 24:1188–1194, 2005.
- [39] Y. Shapira, A. Sagie, R. Jortner, Y. Adler, and R. Hirsch. Thrombosis of bileaflet tricuspid valve prosthesis: clinical spectrum and the role of nonsurgical treatment. *American Heart Journal*, 137:721–725, 1999.
- [40] J. Soulis, G. Giannoglou, Y. Chatzizisis, K. Seralidou, G. Parcharidis, and G. Louridas. Non-newtonian models for molecular viscosity and wall shear stress in a 3d reconstructed human left coronary artery. *Medical engineering & physics*, 30(1):9–19, 2008.
- [41] V. Turitto and H. Baumgartner. Platelet interaction with subendothelium in a perfusion system: physical role of red blood cells. *Microvascular Research*, 9(3):335–344, 1975.
- [42] F. Walburn and D. Schneck. A constitutive equation for whole human blood. *Biorheology*, 13(3):201, 1976.
- [43] M. Wilhelm, D. Hammel, C. Schmid, A. Rhode, T. Kaan, M. Rothenburger, J. Stypmann, M. Schafers, C. Schmidt, H. Baba, et al. Long-term support of 9 patients with the debakey vad for more than 200 days. *Journal of thoracic and cardiovascular surgery*, 130:1122–1129, 2005.
- [44] W. Wilkinson. *Non-Newtonian Fluids*. Pergamon Press, Oxford, 1960.
- [45] A. Zydney, J. Oliver III, and C. Colton. A constitutive equation for the viscosity of stored red cell suspensions: Effect of hematocrit, shear rate, and suspending phase. *Journal of Rheology*, 35:1639, 1991.